developmental potential, even before their physical disappearance. The role of CRL4[VPRBP] in mammalian oocytes is summarized in Fig. 4E.

Although CRL4[VPRBP] is crucial for TET activities, our results suggest that TET1, 2, and 3 are not the only CRL4[VPRBP] substrates in oocytes. More than one-third of the embryos derived from TET3-deleted oocytes could develop to term (11). However, all embryos that were derived from DDB1-deleted oocytes died before the eight-cell stage, which indicated that they had defects other than TET3-mediated genome reprogramming. CRL4 might also recruit other substrate adaptors, poly-ubiquitinate a number of protein substrates, and direct them toward degradation. Identifying other CRL4[VPRBP] substrates will shed new light on the molecular regulatory mechanisms of oocyte functions.

## References and Notes

1. D. Adhikari, K. Liu, Endocr. Rev. 30, 438–464 (2009).
2. S. Jackson, Y. Xiong, Trends Biochem. Sci. 34, 562–570 (2009).
3. S. Angers et al., Nature 443, 590–593 (2006).
4. S. A. Pangas et al., Proc. Natl. Acad. Sci. U.S.A. 103, 8090–8095 (2006).
5. Y. Choi, D. Yuan, A. Rajkovic, Biol. Reprod. 79, 1176–1182 (2008).
6. A. Rajkovic, S. A. Pangas, D. Ballow, N. Suzumori, M. M. Matzuk, Science 305, 1157–1159 (2004).
7. S. M. Soyal, A. Amleh, J. Dean, Development 127, 4645–4654 (2000).
8. J. J. Eppig, Reproduction 122, 829–838 (2001).
9. Y. F. He et al., Science 333, 1303–1307 (2011).
10. S. Ito et al., Science 333, 1300–1303 (2011).
11. T. P. Gu et al., Nature 477, 606–610 (2011).
12. D. H. Castrillon, L. Miao, R. Kollipara, J. W. Horner, R. A. DePinho, Science 301, 215–218 (2003).
13. P. Reddy et al., Hum. Mol. Genet. 18, 2813–2824 (2009).
14. P. Reddy et al., Science 319, 611–613 (2008).

# Serial Femtosecond Crystallography of G Protein–Coupled Receptors

Wei Liu,[1] Daniel Wacker,[1] Cornelius Gati,[2] Gye Won Han,[1] Daniel James,[3] Dingjie Wang,[3] Garrett Nelson,[3] Uwe Weierstall,[3] Vsevolod Katritch,[1] Anton Barty,[2] Nadia A. Zatsepin,[3] Dianfan Li,[4] Marc Messerschmidt,[5] Sébastien Boutet,[5] Garth J. Williams,[5] Jason E. Koglin,[5] M. Marvin Seibert,[5,6] Chong Wang,[1] Syed T. A. Shah,[4] Shibom Basu,[7] Raimund Fromme,[7] Christopher Kupitz,[7] Kimberley N. Rendek,[7] Ingo Grotjohann,[7] Petra Fromme,[7] Richard A. Kirian,[2,3] Kenneth R. Beyerlein,[2] Thomas A. White,[2] Henry N. Chapman,[2,8,9] Martin Caffrey,[4] John C. H. Spence,[3] Raymond C. Stevens,[1] Vadim Cherezov[1]*

X-ray crystallography of G protein–coupled receptors and other membrane proteins is hampered by difficulties associated with growing sufficiently large crystals that withstand radiation damage and yield high-resolution data at synchrotron sources. We used an x-ray free-electron laser (XFEL) with individual 50-femtosecond-duration x-ray pulses to minimize radiation damage and obtained a high-resolution room-temperature structure of a human serotonin receptor using sub-10-micrometer microcrystals grown in a membrane mimetic matrix known as lipidic cubic phase. Compared with the structure solved by using traditional microcrystallography from cryo-cooled crystals of about two orders of magnitude larger volume, the room-temperature XFEL structure displays a distinct distribution of thermal motions and conformations of residues that likely more accurately represent the receptor structure and dynamics in a cellular environment.

G protein–coupled receptors (GPCRs) represent a highly diverse superfamily of eukaryotic membrane proteins that mediate cellular communication. In humans, ~800 GPCRs respond to a variety of extracellular signaling molecules and transmit signals inside the cell by coupling to heterotrimeric G proteins and other effectors. Their involvement in key physiological and sensory processes in humans makes GPCRs prominent drug targets. Despite the high biomedical relevance and decades of dedicated research, knowledge of the structural mechanisms of ligand recognition, receptor activation, and signaling in this broad family remains limited. Challenges for GPCR structural studies include low-expression yields, low receptor stability after detergent extraction from native membranes, and high conformational heterogeneity. Many years of developments aimed at receptor stabilization, crystallization, and microcrystallography culminated in a series of breakthroughs in GPCR structural biology leading to the structure determination of 22 receptors, some of which were solved in several conformational states and one in complex with its G protein partner (1–5).

Nonetheless, crystallographic studies of GPCRs remain difficult because many of them produce only microcrystals. Most GPCR structures to date have been obtained by using crystallization from the membrane-mimetic environment of a lipidic cubic phase (LCP) (6, 7). LCP crystallization has proven successful for obtaining high-resolution structures of a variety of membrane proteins, including ion channels, transporters, and enzymes, in addition to GPCRs (8, 9). This method leads to highly ordered crystals that are, however, often limited in size. Microfocus x-ray beams of high intensity (~$10^9$ photons/s/$\mu m^2$) and long exposures (~5 s) are typically required in order to obtain sufficient intensity for high-resolution data from weakly diffracting microcrystals. The high-radiation doses induce severe radiation damage and require merging data from multiple crystals in order to obtain complete data sets of sufficient quality. Accordingly, sub-10-$\mu m$ GPCR crystals are currently not suitable for high-resolution data collection, even at the most powerful synchrotron microfocus beamlines (7, 10).

Serial femtosecond crystallography (SFX) (11), which takes advantage of x-ray free-electron lasers (XFEL), has recently demonstrated great promise for obtaining room-temperature high-resolution data from micrometer- and sub-micrometer–size crystals of soluble proteins, with minimal radiation damage (12, 13). The highly intense (~2 mJ, $10^{12}$ photons per pulse) and ultrashort (<50 fs) x-ray pulses produced by XFELs enable the recording of high-resolution diffraction snapshots from individual crystals at single orientations before their destruction. SFX data collection, therefore, relies on a continuous supply of small crystals intersecting the XFEL beam in random orientations—typically provided by a fast-running liquid microjet (12)—which is incompatible with streaming highly viscous gel-like materials such as LCP and requires tens to hundreds of milligrams of crystallized protein for data collection (11). For many membrane proteins, including most human membrane proteins, obtaining such quantities is not practical.

[1]Department of Integrative Structural and Computational Biology, The Scripps Research Institute, La Jolla, CA 92037, USA. [2]Center for Free Electron Laser Science, Deutsches Elektronen-Synchrotron, 22607 Hamburg, Germany. [3]Department of Physics, Arizona State University, Tempe, AZ 85287, USA. [4]School of Medicine and School of Biochemistry and Immunology, Trinity College, Dublin, Dublin 2, Ireland. [5]SLAC National Accelerator Laboratory, 2575 Sand Hill Road, Menlo Park, CA 94025, USA. [6]Laboratory of Molecular Biophysics, Department of Cell and Molecular Biology, Uppsala University, Husargatan 3, Box 596, SE-751 24 Uppsala, Sweden. [7]Department of Chemistry and Biochemistry, Arizona State University, Tempe, AZ 85287, USA. [8]Department of Physics, University of Hamburg, 22761 Hamburg, Germany. [9]Center for Ultrafast Imaging, 22607 Hamburg, Germany.

*Corresponding author. E-mail: vcherezo@scripps.edu

We have modified the SFX data collection approach (Fig. 1) and obtained a room-temperature GPCR structure at 2.8 Å resolution using only 300 μg of protein crystallized in LCP. SFX experiments were performed at the Coherent X-ray Imaging (CXI) instrument of the Linac Coherent Light Source (LCLS) [14]. LCP-grown microcrystals (average size of 5 by 5 by 5 μm) (fig. S1) [15] of the human serotonin 5-HT$_{2B}$ receptor [16] bound to the agonist ergotamine were continuously delivered across a ~1.5-μm-diameter XFEL beam by using a specially designed LCP injector. LCP with randomly distributed crystals was ex-

truded through a 20- to 50-μm capillary into a vacuum chamber ($10^{-4}$ torr) at room temperature (21°C) [17] and a constant flow rate of 50 to 200 nL/min and was stabilized by a co-axial flow of helium or nitrogen gas supplied at 20 to 30 bar. We recorded single-pulse diffraction patterns (fig. S2) using 9.5-keV (1.3 Å) x-ray pulses of 50 fs duration at a 120 Hz repetition rate by means of a Cornell-SLAC pixel array detector (CSPAD) [18] positioned at a distance of 100 mm from the sample. The XFEL beam was attenuated to 3 to 6% so as to avoid detector saturation. The average x-ray pulse energy at the sample was 50 μJ

($3 \times 10^{10}$ photons/pulse), corresponding to a radiation dose of up to 25 megagrays per crystal. A total of 4,217,508 diffraction patterns were collected within 10 hours by using ~100 μL of crystal-loaded LCP, corresponding to ~0.3 mg of protein. Of these patterns, 152,651 were identified as crystal hits (15 or more Bragg peaks) by the processing software Cheetah (http://www.desy.de/~barty/cheetah/), corresponding to a hit rate of 3.6%. Of these crystal hits, 32,819 patterns (21.5%) were successfully indexed and integrated by CrystFEL [19] at 2.8 Å resolution (table S1). The structure was determined through molecular replacement and refined to $R_{work}/R_{free}$ = 22.7/27.0%. Overall, the final structure (fig. S3) has a well-defined density for most residues, including the ligand ergotamine (fig. S4).

We compared the XFEL structure of the 5-HT$_{2B}$ receptor/ergotamine complex (5-HT$_{2B-XFEL}$) with the recently published structure of the same receptor/ligand complex obtained by means of traditional microcrystallography at a synchrotron source [Protein Data Bank (PDB) ID 4IB4; 5-HT$_{2B-SYN}$] [21]. Synchrotron data were collected at 100 K on cryo-cooled crystals of a much larger size (average volume, ~$10^4$ μm$^3$) than those used for the XFEL structure (average volume, ~$10^2$ μm$^3$) (fig. S1). Other differences between data collection protocols are listed in table S1. Both data sets were processed in the same spacegroup C222$_1$, which is expected given the very similar crystallization conditions. However, the lattice parameters for the room-temperature XFEL crystals are slightly longer in the $a$ and $b$ directions and slightly shorter in the $c$ direction, resulting in a 2.1% larger unit cell volume. Concomitant with these lattice changes, we observed a ~2.5° rotation of
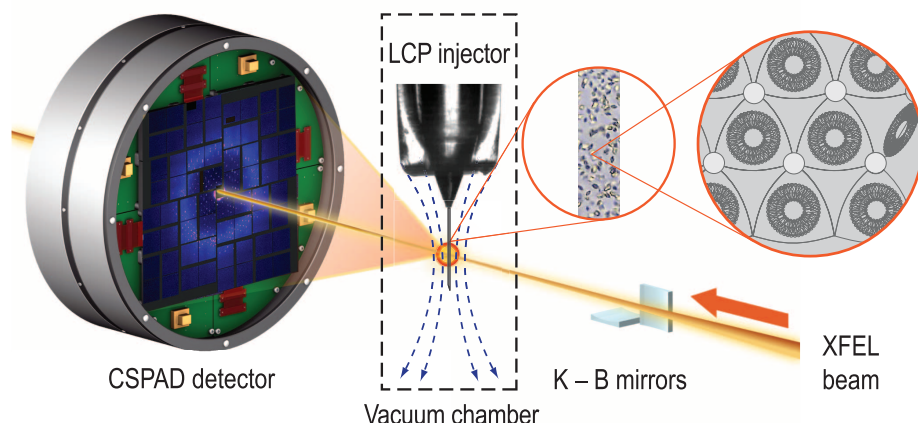


**Fig. 1. Experimental setup for SFX data collection using an LCP injector.** 5-HT$_{2B}$ receptor microcrystals (first zoom level) dispersed in LCP (second zoom level) are injected as a continuous column of 20 to 50 μm in diameter—stabilized by a co-axial gas flow (blue dash curved lines)—inside a vacuum chamber and intersected with 1.5-μm-diameter pulsed XFEL beam focused with Kirkpatrick-Baez (K-B) mirrors. Single-pulse diffraction patterns were collected at 120 Hz by using a CSPAD detector. The entire XFEL beam path and CSPAD are under vacuum.

**Fig. 2. Comparison between 5-HT$_{2B-XFEL}$ (light red) and 5-HT$_{2B-SYN}$ (teal) structures.** Central image represents a backbone overlay of the two structures. Dashed lines correspond to membrane boundaries defined by the Orientation of Proteins in Membrane database (http://opm.phar.umich.edu) [28]. (**A**) Electron density for the Glu212 side chain is missing in 5-HT$_{2B-SYN}$ and fully resolved in 5-HT$_{2B-XFEL}$. (**B**) A salt bridge between Glu319 and Lys247 links intracellular parts of helices V and VI in the 5-HT$_{2B-XFEL}$ structure. In the 5-HT$_{2B-SYN}$ structure, Lys247 makes a hydrogen bond with Tyr1105 from the BRIL fusion protein. (**C**) Extracellular tip of helix II forms a regular helix in 5-HT$_{2B-XFEL}$ with Thr114, making a stabilizing hydrogen bond with the backbone carbonyl, whereas in 5-HT$_{2B-SYN}$, a water-stabilized kink is introduced at this position. (**D**) Tyr87 forms a hydrogen bond with Asn90 in 5-HT$_{2B-XFEL}$; this hydrogen bond is broken, and Tyr87 adopts a different rotamer conformation in the 5-HT$_{2B-SYN}$ structure. 2mF$_{obs}$-DF$_{calc}$ maps (contoured at 1σ level) are shown only around described residues.
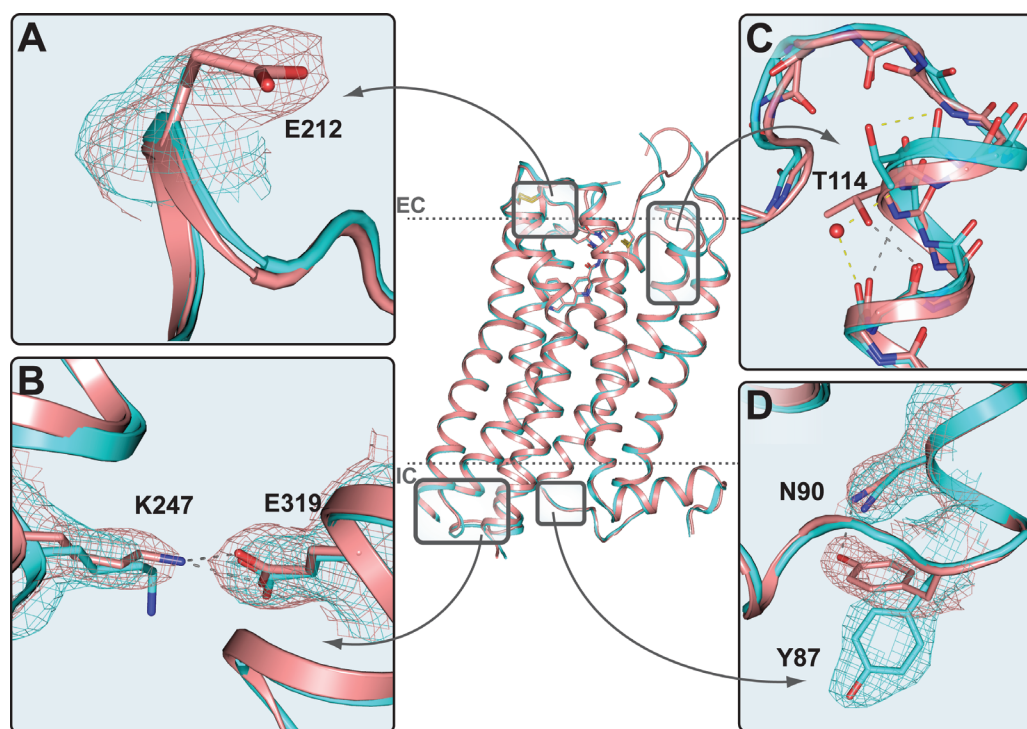
the b$_{562}$ RIL (BRIL) fusion domain with respect to the receptor (fig. S5). Otherwise, the receptor domains of the 5-HT$_{2B-XFEL}$ and 5-HT$_{2B-SYN}$ structures are very similar [receptor Cα root mean square deviation (RMSD) = 0.46 Å, excluding flexible residues at the N terminus, 48 to 51, and in the extracellular loop  2 (ECL2), 195 to 205] (Fig. 2). The ligand ergotamine has indistinguishable electron density and placement (total ligand RMSD = 0.32 Å) in both structures (Fig. 2 and fig. S4B). The largest backbone deviations were observed in the loop regions, especially in the stretch of ECL2 between helix IV and the Cys128–Cys207 disulfide bond, which is apparently very flexible. We observed an unexpected backbone deviation at the extracellular tip of helix II (Fig. 2C), which adopts a regular α-helix in the 5-HT$_{2B-XFEL}$ structure, with Thr$^{114}$ forming a stabilizing hy-

drogen bond with the main chain carbonyl of Ile110. In the 5-HT$_{2B-SYN}$ structure, however, a water-stabilized kink was found at this location, which results in the two structures deviating by 2.0 Å (at Cα atom of Thr114) at the tip of helix II and up to 3.4 Å (at O atom of Phe117) in ECL1.

Although absolute B- (or temperature) factor values can be affected by errors associated with experimental conditions, their distribution generally represents the relative static and dynamic flexibility of the protein in the crystal (22). Because both structures were obtained from similar samples and at similar resolutions, we analyzed their B-factor distributions so as to study the effect of the different temperatures on the thermal motions of the receptor. The average B-factor for the receptor part in the room-temperature 5-HT$_{2B-XFEL}$ structure (88.4 Å$^2$) is 21 Å$^2$ larger than that in the

cryo 5-HT$_{2B-SYN}$ structure (67.2 Å$^2$), which is consistent with larger thermal motions at higher temperature and possible effects of Bragg termination during the XFEL pulse (20). The distribution of B-factors highlights a more rigid core of the seven transmembrane helices in comparison with loops, with more pronounced B-factor deviations observed in the room-temperature 5-HT$_{2B-XFEL}$ structure (Fig. 3 and fig. S6). N terminus, intracellular loop 2 (ICL2), ECL1, and part of ECL2 between helix IV and the Cys128–Cys207 disulfide bond show much larger deviations in B-factors (50 to 100 Å$^2$) between the two structures as compared with the average difference of 21 Å$^2$. These parts of the structure are not involved in direct interactions with the ligand ergotamine, but their mobility may affect the kinetics of ligand binding and interactions with intracellular binding partners (23). In contrast, ICL1, part of ECL2 between the Cys128–Cys207 disulfide bond and helix V, and ECL3 display just an average increase in the B-factors, suggesting that the relative range of their thermal fluctuations was adequately captured in the cryo structure. As previously established with cryocrystallography, one of the most pronounced differences between the two subtypes of serotonin receptors, 5-HT$_{2B}$ and 5-HT$_{1B}$, occurs at the extracellular tip of helix V and ECL2, which forms an additional helical turn stabilized by a water molecule in 5-HT$_{2B}$ (21). This additional turn pulls the extracellular tip of helix V toward the center of the helical bundle and was suggested to be responsible for the biased agonism of ergotamine at the 5-HT$_{2B}$ receptor. The 5-HT$_{2B-XFEL}$ structure confirms the rigid structured conformation of ECL2, stabilized by a comprehensive network of hydrogen bonds, involving residues Lys193, Glu196, Arg213, Asp216, and a lipid OLC (monoolein) (fig. S7); however, no ordered water molecule was observed, emphasizing that water is more disordered and probably does not play a substantial structural role at this location.

Several side chains have partly missing electron density in both room-temperature and cryo structures (table S2). Such lack of density is most likely related to disorder of the corresponding side chains (such as residues at the N terminus, ECL2, and ICL2) (Fig. 2A). Two disulfide bonds, Cys128–Cys207 and Cys350–Cys353, are intact and well resolved in both structures; however, the B-factor increase in the 5-HT$_{2B-XFEL}$ structure compared with 5-HT$_{2B-SYN}$ for each of these disulfide bonds (11.1 and 5.7 Å$^2$, respectively) is lower than that of the average B-factor increase (21 Å$^2$). Several side chains have different rotamer conformations between the two structures (Fig. 2D and table S3), which is consistent with a partial remodeling of the side chain conformational distribution upon cryo-cooling observed in soluble proteins (24). Several interactions involving charged residues appear stronger and better defined in 5-HT$_{2B-XFEL}$ compared with the 5-HT$_{2B-SYN}$ structure (table S4). This strengthening of the charged interactions at higher temperatures potentially can be explained
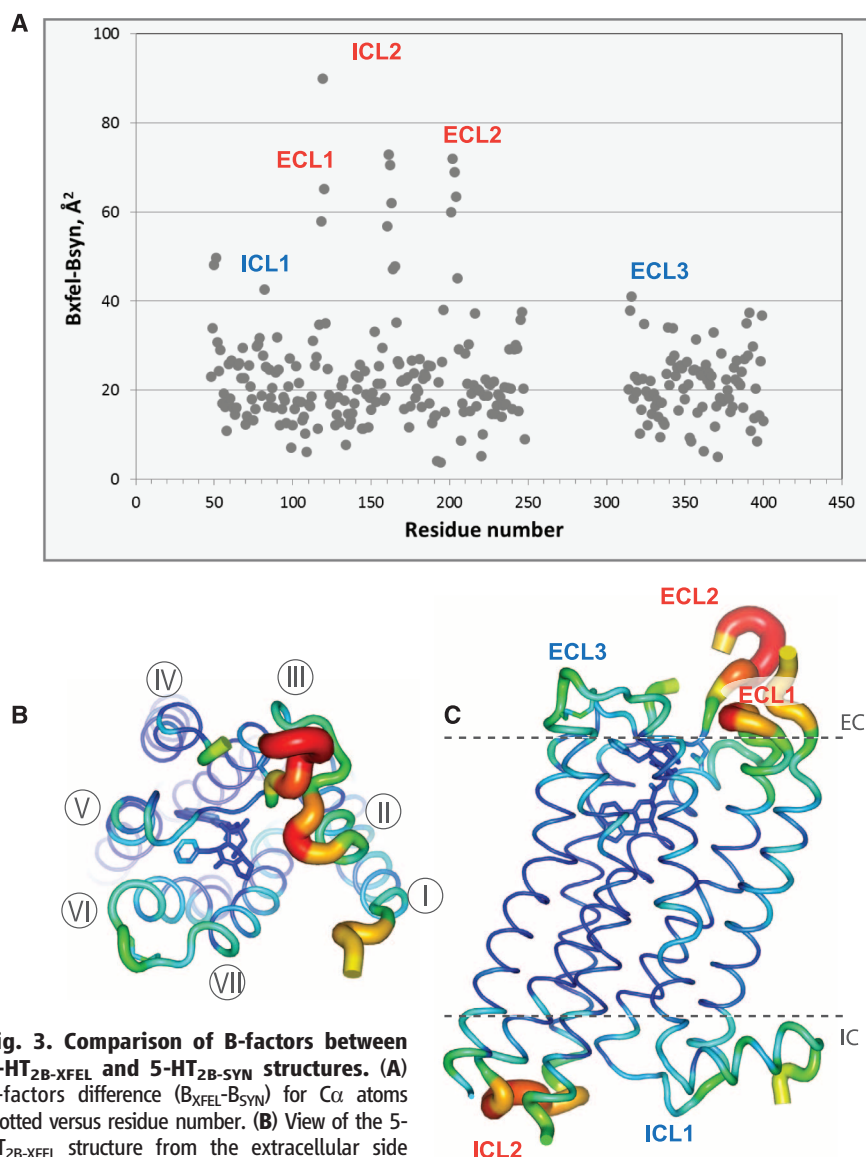


**Fig. 3. Comparison of B-factors between 5-HT$_{2B-XFEL}$ and 5-HT$_{2B-SYN}$ structures.** (A) B-factors difference (B$_{XFEL}$-B$_{SYN}$) for Cα atoms plotted versus residue number. (B) View of the 5-HT$_{2B-XFEL}$ structure from the extracellular side and (C) in the lateral-to-membrane orientation. Structure in (B) and (C) is shown in putty representation and colored in rainbow colors by the Cα B-factors (range 60 to 170 Å$^2$). Loops for which the B-factor difference is above 50 Å$^2$ are labeled in red, and those with a difference below 50 Å$^2$ are in blue in (A) and (C). Helices are labeled in (B).

by a decrease in the dielectric constant of water with temperature, reducing the desolvation penalty (25, 26). In particular, the salt bridge between Glu319 and Lys247 is well defined in the 5-HT$_{2B-XFEL}$ structure but appears broken in the cryo 5-HT$_{2B-SYN}$ structure (Fig. 2B). Because GPCR activation has been associated with large-scale structural changes in the intracellular parts of helices V and VI, this salt bridge may play a role in the receptor function and is likely to be more accurately resolved and represented in the 5-HT$_{2B-XFEL}$ structure recorded at room temperature.

Overall, the observed differences likely originate from effects related to thermal motions, cryo-cooling (24), and radiation damage (27). Thus, the XFEL source enables access to a room-temperature GPCR structure, which more accurately represents the conformational ensemble for this receptor under native conditions. Because dynamics are an integral part of GPCR biology, the use of SFX to accurately determine GPCR structural details at room temperature can make an important contribution to understanding the structure-function relationships in this superfamily.

### References and Notes

1. V. Cherezov et al., Science 318, 1258–1265 (2007).
2. S. G. Rasmussen et al., Nature 469, 175–180 (2011).
3. V. Katritch, V. Cherezov, R. C. Stevens, Annu. Rev. Pharmacol. Toxicol. 53, 531–556 (2013).
4. A. J. Venkatakrishnan et al., Nature 494, 185–194 (2013).
5. M. Audet, M. Bouvier, Cell 151, 14–23 (2012).
6. E. M. Landau, J. P. Rosenbusch, Proc. Natl. Acad. Sci. U.S.A. 93, 14532–14535 (1996).
7. M. Caffrey, V. Cherezov, Nat. Protoc. 4, 706–731 (2009).
8. V. Cherezov, Curr. Opin. Struct. Biol. 21, 559–566 (2011).
9. M. Caffrey, D. Li, A. Dukkipati, Biochemistry 51, 6266–6288 (2012).
10. J. L. Smith, R. F. Fischetti, M. Yamamoto, Curr. Opin. Struct. Biol. 22, 602–612 (2012).
11. H. N. Chapman et al., Nature 470, 73–77 (2011).
12. S. Boutet et al., Science 337, 362–364 (2012).
13. L. Redecke et al., Science 339, 227–230 (2013).
14. S. Boutet, G. J. Williams, New J. Phys. 12, 035024 (2010).
15. Materials and methods are available as supplementary materials on Science Online.
16. The engineered-for-crystallization construct is based on the sequence of the human 5-HT$_{2B}$ receptor with the following modifications: (i) Residues Tyr249–Val313 within ICL3 were replaced with Ala1–Leu106 of thermostabilized apo cytochrome BRIL; (ii) N-terminal residues 1 to 35 and C-terminal residues 406 to 481 were truncated; and (iii) a thermostabilizing Met144 Trp mutation was introduced.
17. The temperature measured in the CXI hutch during the experiments was 294 K (21°C). The actual crystal temperature was likely a few degrees lower because of the evaporative cooling upon injection of crystal-loaded LCP in vacuum.
18. P. Hart et al., Proc. SPIE 8504, 85040C (2012).
19. T. A. White et al., Acta Crystallogr. D Biol. Crystallogr. 69, 1231–1240 (2013).
20. A. Barty et al., Nat. Photonics 6, 35–40 (2012).
21. D. Wacker et al., Science 340, 615–619 (2013).
22. B. T. M. Willis, A. W. Pryor, Thermal Vibrations in Crystallography (Cambridge Univ. Press, London, 1975).
23. A. C. Pan, D. W. Borhani, R. O. Dror, D. E. Shaw, Drug Discov. Today 18, 667–673 (2013).
24. J. S. Fraser et al., Proc. Natl. Acad. Sci. U.S.A. 108, 16247–16252 (2011).
25. A. H. Elcock, J. Mol. Biol. 284, 489–502 (1998).
26. S. Kumar, R. Nussinov, ChemBioChem 3, 604–617 (2002).
27. E. F. Garman, Acta Crystallogr. D Biol. Crystallogr. 66, 339–351 (2010).
28. M. A. Lomize, A. L. Lomize, I. D. Pogozheva, H. I. Mosberg, Bioinformatics 22, 623–625 (2006).

# mTOR Inhibition Alleviates Mitochondrial Disease in a Mouse Model of Leigh Syndrome

Simon C. Johnson,[1] Melana E. Yanos,[1,2] Ernst-Bernhard Kayser,[3] Albert Quintana,[4] Maya Sangesland,[1] Anthony Castanza,[1] Lauren Uhde,[1] Jessica Hui,[1] Valerie Z. Wall,[1] Arni Gagnidze,[1] Kelly Oh,[1] Brian M. Wasko,[1] Fresnida J. Ramos,[1] Richard D. Palmiter,[4] Peter S. Rabinovitch,[1] Philip G. Morgan,[3] Margaret M. Sedensky,[3] Matt Kaeberlein[1]*

Mitochondrial dysfunction contributes to numerous health problems, including neurological and muscular degeneration, cardiomyopathies, cancer, diabetes, and pathologies of aging. Severe mitochondrial defects can result in childhood disorders such as Leigh syndrome, for which there are no effective therapies. We found that rapamycin, a specific inhibitor of the mechanistic target of rapamycin (mTOR) signaling pathway, robustly enhances survival and attenuates disease progression in a mouse model of Leigh syndrome. Administration of rapamycin to these mice, which are deficient in the mitochondrial respiratory chain subunit Ndufs4 [NADH dehydrogenase (ubiquinone) Fe-S protein 4], delays onset of neurological symptoms, reduces neuroinflammation, and prevents brain lesions. Although the precise mechanism of rescue remains to be determined, rapamycin induces a metabolic shift toward amino acid catabolism and away from glycolysis, alleviating the buildup of glycolytic intermediates. This therapeutic strategy may prove relevant for a broad range of mitochondrial diseases.

Leigh syndrome is a clinically defined disease resulting from genetic defects that disrupt mitochondrial function. It is the most common childhood mitochondrial disorder, affecting 1 in 40,000 newborns in the United States (1). Leigh syndrome is characterized by

# Science

## Serial Femtosecond Crystallography of G Protein−Coupled Receptors

Wei Liu, Daniel Wacker, Cornelius Gati, Gye Won Han, Daniel James, Dingjie Wang, Garrett Nelson, Uwe Weierstall, Vsevolod Katritch, Anton Barty, Nadia A. Zatsepin, Dianfan Li, Marc Messerschmidt, Sébastien Boutet, Garth J. Williams, Jason E. Koglin, M. Marvin Seibert, Chong Wang, Syed T. A. Shah, Shibom Basu, Raimund Fromme, Christopher Kupitz, Kimberley N. Rendek, Ingo Grotjohann, Petra Fromme, Richard A. Kirian, Kenneth R. Beyerlein, Thomas A. White, Henry N. Chapman, Martin Caffrey, John C. H. Spence, Raymond C. Stevens and Vadim Cherezov

### G Structures

G protein−coupled receptors (GPCRs) are eukaryotic membrane proteins that have a central role in cellular communication and have become key drug targets. To overcome the difficulties of growing GPCRs crystals, **Liu *et al.*** (p. 1521) used an x-ray free-electron laser to determine a high-resolution structure of the serotonin receptor from microcrystals.

| | |
|---|---|
| ARTICLE TOOLS | http://science.sciencemag.org/content/342/6165/1521 |
| SUPPLEMENTARY MATERIALS | http://science.sciencemag.org/content/suppl/2013/12/19/342.6165.1521.DC1 |
| RELATED CONTENT | http://stke.sciencemag.org/content/sigtrans/7/307/ec4.abstract |
| REFERENCES | This article cites 36 articles, 7 of which you can access for free http://science.sciencemag.org/content/342/6165/1521#BIBL |
| PERMISSIONS | http://www.sciencemag.org/help/reprints-and-permissions |

Use of this article is subject to the Terms of Service